Int. J. Heat Mass Transfer. Vol. 31, No. 1, pp. 107–118, 1988
Printed in Great Britain

0017–9310/88 $3.00 + 0.00

Numerical simulation of forced convection heat transfer from a cylinder in crossflow

GEORGE EM KARNIADAKIS
Department of Mechanical Engineering, Massachusetts Institute of Technology, Cambridge, MA 02139, U.S.A.

(*Received* 20 *January* 1987 *and in final form* 24 *June* 1987)

Abstract—Forced convection heat transfer from an isolated cylinder in crossflow is investigated for Reynolds numbers up to 200 by direct numerical simulation of the Navier–Stokes and energy equations using the spectral element method. The numerical predictions for the size of the wake, the temporal and spatial structure of the von Karman vortex street, the unsteady lift and drag coefficient, and the unsteady local heat transfer coefficient are all in excellent agreement with available experimental data. Various outflow boundary conditions for the velocity field are employed to account for the unboundedness of the domain, while for the temperature field the conditions of uniform heat flux and constant cylinder temperature are simulated.

INTRODUCTION

THE FLOW past a circular cylinder has long been a model for fundamental studies of challenging fluid mechanics problems, as well as representing an important class of engineering applications. Beginning with the work of Bènard (1908) [1], von Karman (1911) [2] and Nayler and Frayzer (1917) [3] on the development of the vortex street, many studies of the cylinder flow problem have been undertaken. As regards heat transfer, Schmidt and Wenner [4] were the first to report on local transport rates from the cylinder surface. Since then, numerous experimental results and empirical correlations for the heat transfer and drag on the cylinder have been reported in the literature [5–10]. However, to our knowledge, no accurate numerical predictions for unsteady heat transfer have appeared yet.

In this paper, we present results of numerical simulation of the unsteady Navier–Stokes and energy equations for laminar two-dimensional flow past a circular cylinder. The numerical results are obtained using a general-purpose spectral element code, NEKTON [11]. The purpose of the work is twofold: (1) to achieve a relatively complete set of (experimentally validated) numerical results for low to moderate Reynolds number bluff body heat transfer; (2) to demonstrate the accuracy of the spectral element method [12–14]. As regards the latter, the problem of flow past a cylinder serves as a severe test of a numerical method due to the unbounded domain and the highly unsteady nature of the flow field. Furthermore, correct prediction of local transport rates requires resolution of both the (fore) boundary layer and (aft) wake structure of the near cylinder flow.

PROBLEM FORMULATION AND NUMERICAL METHODS

We consider here flow past a cylinder in the domain depicted in Fig. 1. The momentum, continuity and energy equations governing the flow are given by

$$\mathbf{v}_t = \mathbf{v}x\boldsymbol{\omega} - \nabla\Pi + Re^{-1}\nabla^2\mathbf{v} \tag{1a}$$

$$\nabla\cdot\mathbf{v} = 0 \tag{1b}$$

$$T_t + \nabla\cdot(\mathbf{v}T) = (Re\,Pr)^{-1}\nabla^2 T \tag{1c}$$

respectively, where $\mathbf{v}(x)$ $(=u\hat{x}+v\hat{y})$ is the velocity, $T(x)$ the temperature, ω the vorticity, $\boldsymbol{\omega} = \nabla x\mathbf{v}$, $\Pi = p + 1/2\mathbf{v}\cdot\mathbf{v}$ the dynamic pressure, $Re = U_\infty D/\nu$ the Reynolds number, and $Pr = \nu/\alpha$ the Prandtl number. Here U_∞ is the freestream velocity, D the cylinder diameter, ν the kinematic viscosity of the fluid and α the thermal diffusivity. All velocities and lengths are scaled by U_∞ and by the cylinder radius R, respectively.

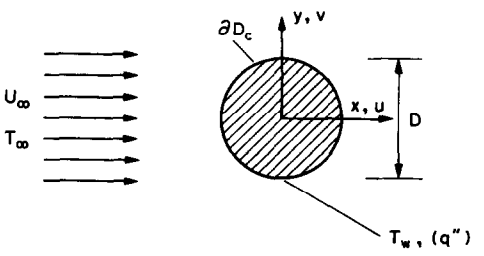

FIG. 1. Geometry definition for flow past a cylinder in an unbounded domain.

NOMENCLATURE

C_D	drag coefficient, $F_D/(1/2\rho U_\infty^2 D)$
C_L	lift coefficient, $F_L/(1/2\rho U_\infty^2 D)$
D	cylinder diameter
f	shedding frequency
F_D	cylinder drag force
F_L	cylinder lift force
h	heat transfer coefficient
k	thermal conductivity
L	wake length
Nu	Nusselt number, $q'' D/(k\Delta T)$
$Nu_{x,I}$	time-averaged Nusselt number
$Nu_{\bar{x},I}$	space- and time-averaged Nusselt number
p	static pressure
Pr	Prandtl number, ν/α
q''	cylinder heat flux
R	cylinder radius
Re	Reynolds number, $U_\infty D/\nu$
St	Strouhal number, fD/U_∞
t	non-dimensional time, R/U_∞
T	temperature
ΔT	temperature difference, $T_w - T_\infty$
U_∞	freestream velocity
$\mathbf{v}$	velocity vector, $u\hat{x}+v\hat{y}$.

Greek symbols

θ	non-dimensional temperature, $(T-T_\infty)/\Delta T$ or $(T-T_\infty)k/(q''R)$
ν	kinematic viscosity
Π	dynamic pressure
ρ	density
τ	time period of vortex shedding
ω	vorticity.

The boundary conditions on $\mathbf{v}$ are

$$\mathbf{v} = 0 \quad \text{on} \quad \partial D_c \tag{2a}$$

$$\mathbf{v} \Rightarrow U_\infty \hat{x} \quad \text{as} \quad |x| \Rightarrow \infty \tag{2b}$$

where ∂D_c is the cylinder surface. For the temperature we impose either

$$\theta = 1 \quad \text{on} \quad \partial D_c \tag{3a}$$

$$\theta \Rightarrow 0 \quad \text{as} \quad |x| \Rightarrow \infty \tag{3b}$$

or

$$\nabla\theta \cdot \hat{n} = 1 \quad \text{on} \quad \partial D_c \tag{4a}$$

$$\theta \Rightarrow 0 \quad \text{as} \quad |x| \Rightarrow \infty \tag{4b}$$

with $\theta = (T-T_\infty)/(T_w - T_\infty)$ and $(T-T_\infty)k/(q''R)$ in equations (3) and (4), respectively. Equation (3) corresponds to imposed constant cylinder temperature, whereas equation (4) represents a constant flux boundary condition. Here T_w is the cylinder temperature, T_∞ the temperature at infinity, q'' the flux at the cylinder surface, and k the thermal conductivity of the fluid.

To solve the above equations numerically, we use the general purpose code NEKTON [11], which is based on the spectral element method. The isoparametric spectral element method [12–14] is a high-order technique that combines the accuracy of spectral methods with the geometric flexibility of finite element schemes. In the spectral element discretization, the domain is broken up into general, four-sided (quadrangular) elements and the geometry, velocity, pressure, and temperature are represented as high-order Lagrangian interpolants through Chebyshev or Legendre collocation points. The integration proceeds by treating the non-linear terms explicitly in time (third-order Adams–Bashforth) with collocation in space, followed by implicit treatment of the pressure and viscous terms using standard variational spatial projection operators.

The spectral element method is a technique particularly appropriate for direct simulations of unsteady and transitional flows, due to its rapid (exponential) convergence, good resolution properties, and minimal numerical dispersion and diffusion. A typical spectral element mesh for our cylinder calculations is shown in Fig. 2, where it can be seen that very high resolution is placed near the cylinder in order to resolve the momentum and thermal boundary layer. The boundary conditions on the computational mesh are taken to be uniform oncoming flow, potential flow at side 'walls', no-slip on the cylinder walls, and outflow Neumann conditions ($\partial \cdot / \partial n = 0$, where n denotes normal to the boundary direction) at the downstream boundary. Various

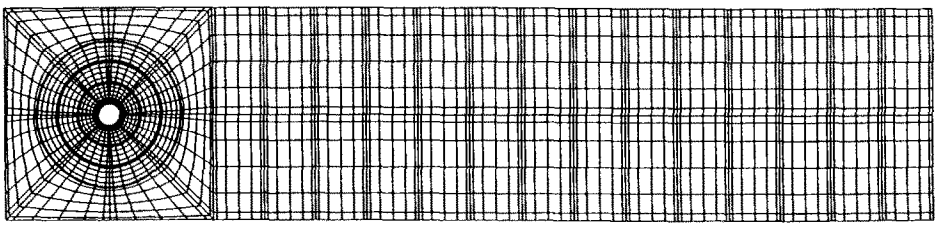

FIG. 2. A typical spectral element mesh. Notice the flexible resolution of the elemental decomposition.

experiments were carried out to verify the mesh independence of the solution and different boundary conditions at the truncation of the infinite domain were employed. The results in all cases were found to differ by less than 1%.

RESULTS AND DISCUSSION

Steady state flow

For Reynolds numbers less than approximately 40 the cylinder flow is steady and takes the form of an attached pair of vortices behind the cylinder. In Figs. 3 and 4 we compare our results to previous experimental [15] and numerical results [16] for the transient development of the vortices (impulsive start), and steady state wake length, respectively. In both cases the agreement is excellent. At $Re = 40$ the wake flow is already unstable far downstream but a pair of vortices remains attached to the cylinder surface.

Vortex shedding

A typical streamline pattern of the unsteady flow, which occurs for a Reynolds number greater than 40, is presented in Fig. 5 at a Reynolds number of 150 every $\tau/3$, where τ is the period of natural shedding. In Fig. 6(a) instantaneous velocity profiles in the circumferential direction for $Re = 200$ are plotted at different positions along the cylinder periphery corresponding to a velocity field depicted in Fig. 6(b) as a streamline plot. The good resolution of the thin boundary layers is clearly demonstrated (the boundary layer thickness is approximately 8% of the cylinder diameter at this Reynolds number). In Table 1 a summary of the predicted shedding frequency (Strouhal number, fD/U_∞) is given for the Reynolds numbers studied, along with the available experimental and numerical results from previous studies [17, 18].

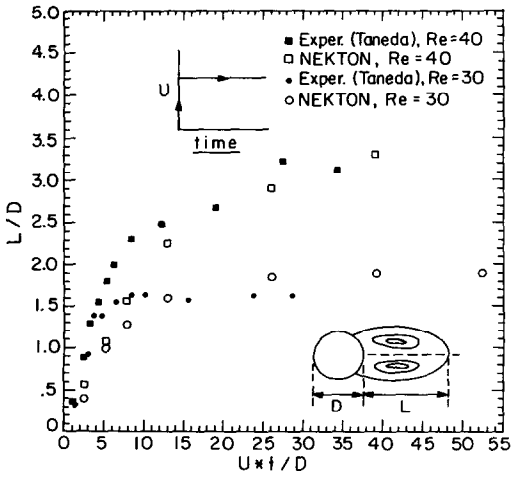

FIG. 3. Comparison of predicted wake length vs dimensionless time for $Re = 30$, 40 with experiment [15].

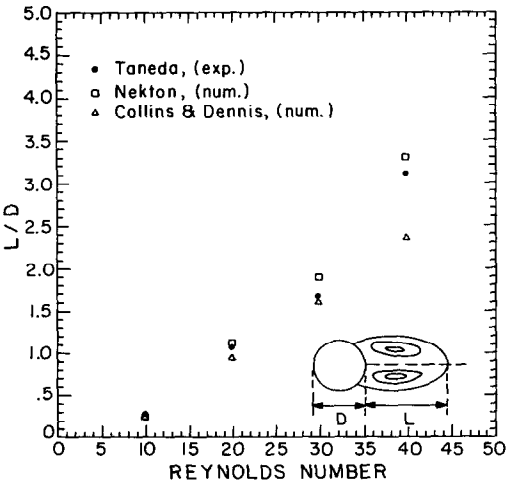

FIG. 4. Wake length vs Reynolds number. Comparison with experiment [15] and another numerical scheme [16].

In Fig. 7(b) the instantaneous temperature field is plotted for $Re = 100$ and $Pr = 2$. The close resemblance of these temperature contours with the streakline photographs obtained experimentally [15, 24] can be seen by comparing Fig. 7(b) with Fig. 7(a). The shape of the vortices and their locations as predicted by NEKTON compare very well with the shape and location of the vortices in the physical experiment, although the visualization mechanisms are somewhat different. The plot of instantaneous isotherms demonstrates the minimal dispersion of the spectral element method [25], and the fact that the method correctly predicts the spatial structure of the von Karman street.

Heat transfer results

In Figs. 8(a)–(c) we plot NEKTON predictions for the local time-averaged Nusselt number $Nu_{x,t} = q''D/(k(T_w - T_\infty))$ for *constant heat flux* conditions (equation (4)) as a function of angle vs Eckert's experimental [19] and numerical [20] results for $Re = 20$, 100 and 200, respectively and $Pr = 0.7$. It should be noted here that Eckert's experimental results are based on an assumption of an empirical relationship between the average Nusselt number and Reynolds number, $Nu = 0.43 + 0.48Re^{1/2}$. This relationship was used in ref. [19] to deduce the Reynolds number from the Nusselt number, since at the time

Table 1

Re	Present work	Gerrard (exp. [17])	Gresho *et al.* (num. [18])
50	0.14	0.14	0.14
100	0.18	0.17	0.18
200	0.20	0.18–0.20	0.22

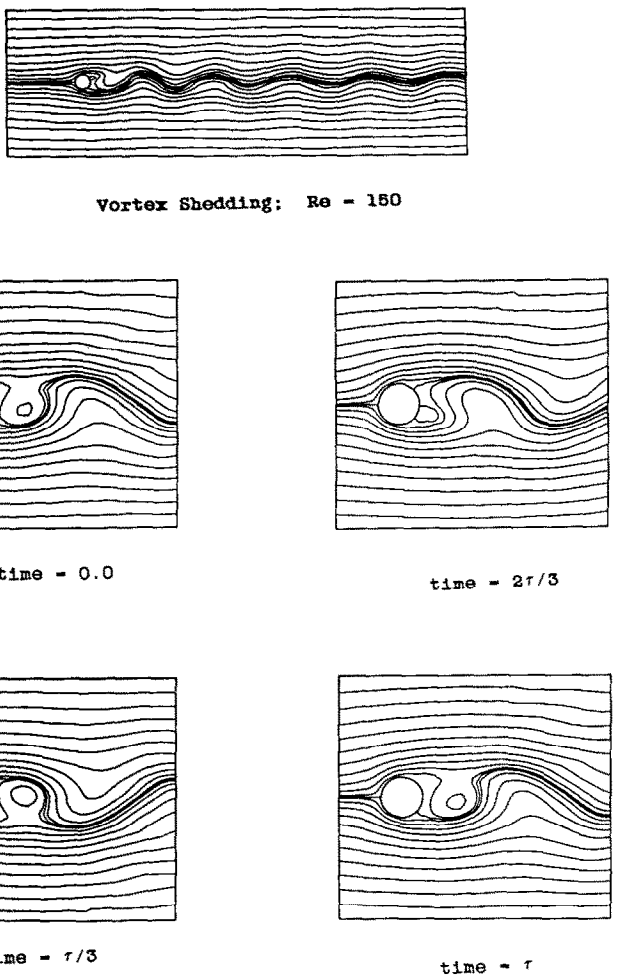

FIG. 5. The von Karman vortex street and details of shedding during a flow cycle for $Re = 150$.

the measurements were made (1953) no instrument was available to measure the low air velocities associated with these Reynolds numbers. This empirical relationship is, in fact, a good approximation only in the front stagnation region of the cylinder, and it is not valid in the wake, where other empirical formulas have been proposed with higher powers of Reynolds number [9]. It is, therefore, expected that the Reynolds number in ref. [19] was overestimated, that is, the Nusselt number measured actually occurs at lower

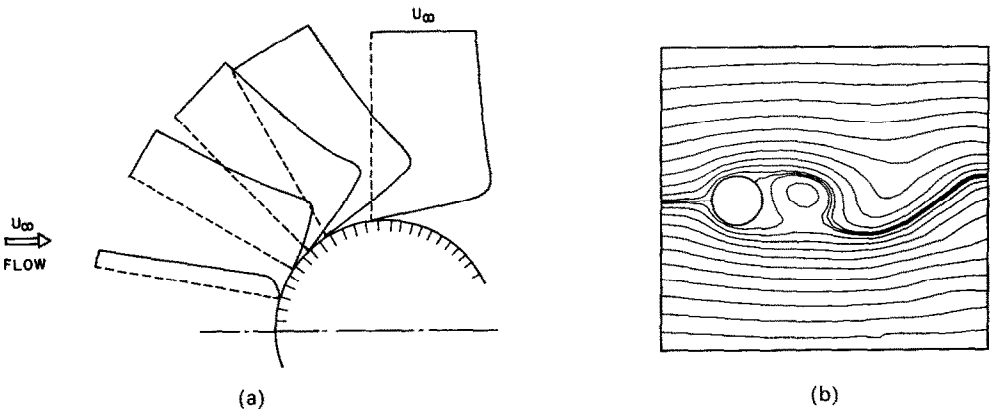

FIG. 6. (a) Instantaneous velocity profiles in circumferential direction for $Re = 200$. The boundary layer is resolved with at least three mesh nodes in all calculations. (b) Corresponding streamline plot.

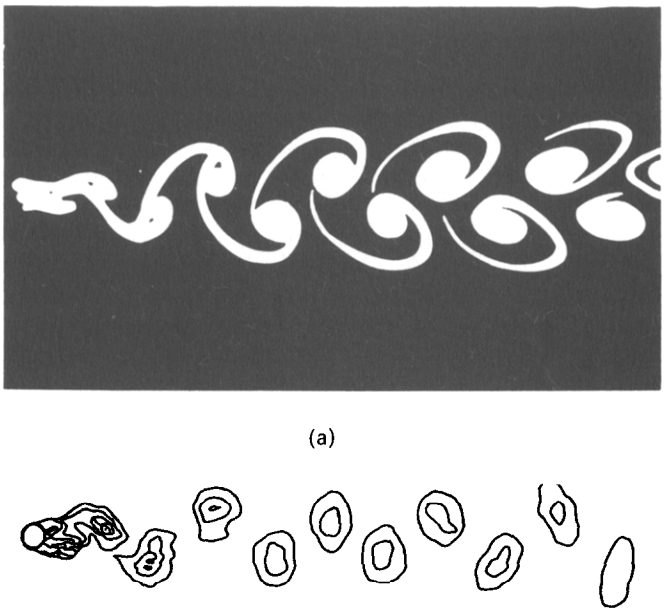

(a)

(b)

FIG. 7. Instantaneous temperature contours for $Re = 100$ and $Pr = 2$. Notice the close resemblance with the photographs from experiments by S. Taneda, *An Album of Fluid Motion*, photograph No. 96 (Ed. Van Dyke).

Reynolds number. This is consistent with the discrepancy in Fig. 8(c).

We also note that the numerical results published by Krall and Eckert in 1970 [20] are based on the assumption of steady flow, which results in overestimation of the Nusselt number in the stagnation region of the flow, and incorrect predictions for the Nusselt number in the wake region of the flow at higher Reynolds numbers. The discrepancy between the NEKTON results and Eckert's steady numerical results is consistent with these facts.

In Fig. 9 the surface temperature, θ, for constant cylinder flux at $Re = 150$ and $Pr = 0.70$ is plotted as a function of time at the rear stagnation point A and at 67.5° from the front stagnation point, at point B. It is seen that the temperature at the stagnation point oscillates twice as fast and corresponds to a larger amplitude. This reflects the fact that the rear stagnation point, being on the cylinder centerline, is influenced by the alternating detachment of vortices from both separation points every $\tau/2$, whereas any other point off the centerline on the cylinder surface is influenced by the detachment of vortices from one separation point only every τ. The temperature field is out of phase with the velocity field but its time history closely follows the time history of the x-component u of the velocity, which also oscillates with $\tau/2$ at the centerline. However, the y-component v of velocity oscillates with period τ everywhere in the flow field and it is, too, out of phase with the x-velocity component. This is demonstrated in Figs. 10(a)–(c), where the x-, y-velocity components u and v and the temperature θ at a point located $0.92D$ downstream of the cylinder and slightly $(0.068D)$ above the centerline are plotted as a function of time for $Re = 150$ and $Pr = 0.7$.

In Fig. 11, we plot the time-averaged circumferential variation of heat transfer coefficient, in the case of *constant cylinder surface temperature*, where very good agreement with the classical results of Schmidt and Wenner ($Re = 31\,000$) [4], and the more recently obtained experimental results can be seen, especially in the wake region of the flow [21]. In Fig. 12 the time- and space-averaged $Nu_{\hat{x},t}$ coefficient is plotted as a function of Reynolds number over the range $0 < Re < 200$ for the constant temperature boundary condition, where it is seen that there is excellent agreement with available correlations [6, 26].

Cylinder drag results

In Fig. 13, the cylinder drag coefficient, $C_D = F_D/(1/2\rho U_\infty^2 D)$, is plotted as a function of Reynolds number and compared with experimental results [22]; again, the agreement is excellent for this range of Reynolds number. Recent numerical data by Braza *et al.* [23] is also in very good agreement with our predictions. In Figs. 14(a) and (b) the two components of the total cylinder drag, namely the viscous and pressure (form) drag coefficients, defined as $F_{D,visc}/(1/2\rho U_\infty^2 D)$ and $F_{D,pres}/(1/2\rho U_\infty^2 D)$, respectively, are plotted as a function of time for a representative case of Reynolds number of 200. Again the presence of different frequency components is observed as compared to the lift coefficient, $C_L = F_L/(1/2\rho U_\infty^2 D)$, in

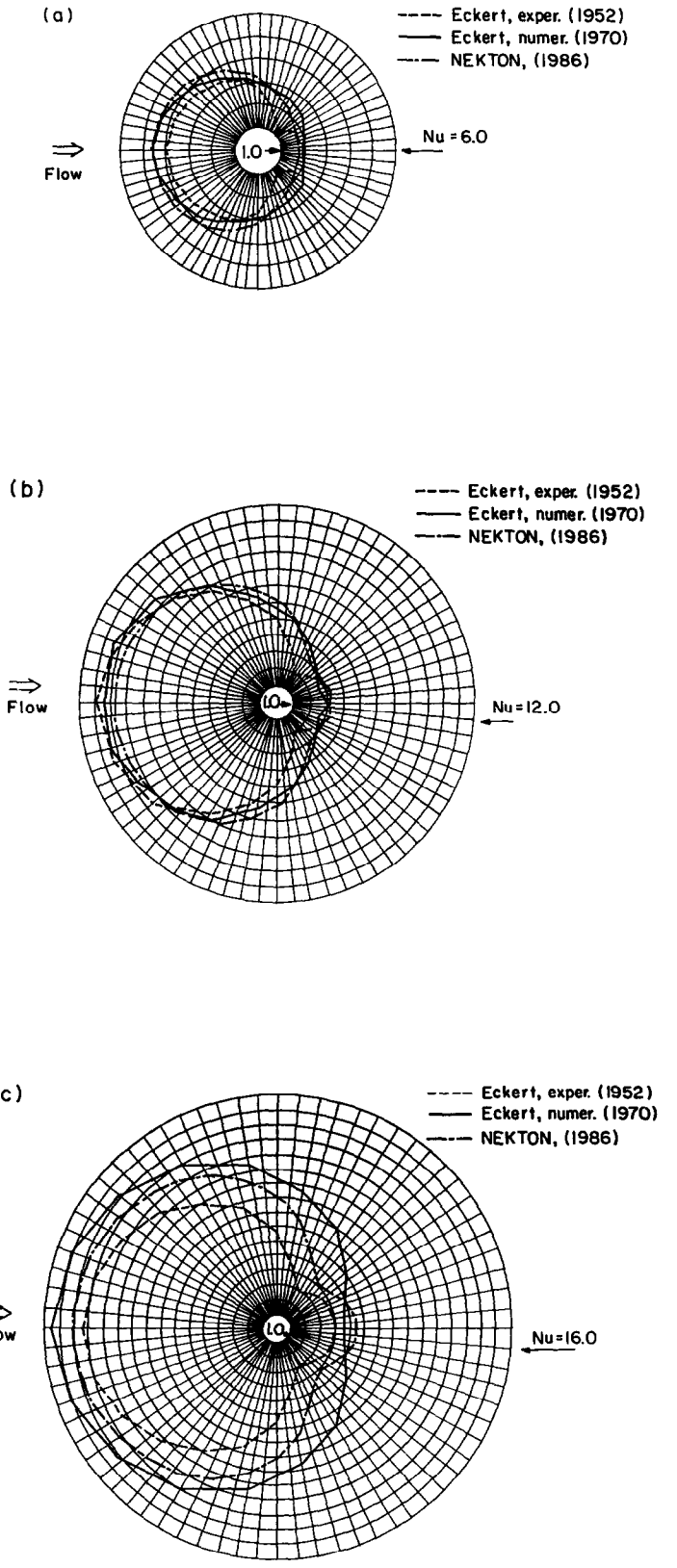

FIG. 8. Predicted local heat transfer distribution around the cylinder surface for constant heat flux compared with Eckert's experimental and numerical results [19, 20]: (a) $Re = 20$, $Pr = 0.70$; (b) $Re = 100$, $Pr = 0.70$; (c) $Re = 200$, $Pr = 0.70$.

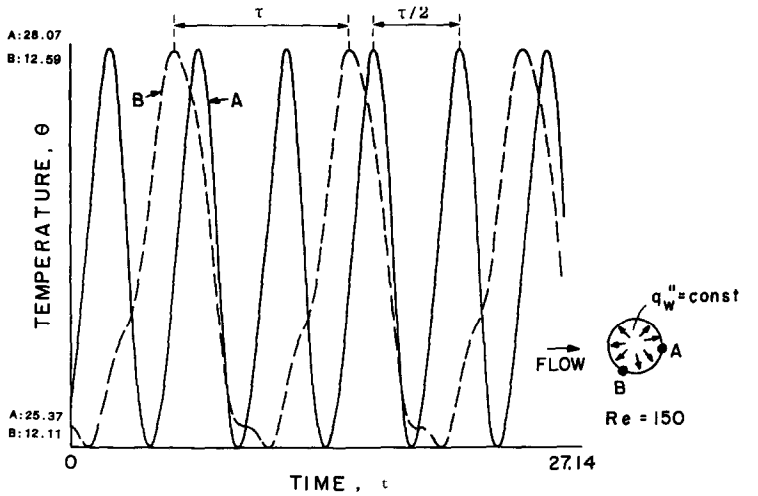

FIG. 9. Cylinder surface temperature for $Re = 200$ and $Pr = 0.70$ as a function of time. Notice the higher harmonics of temperature at the stagnation point.

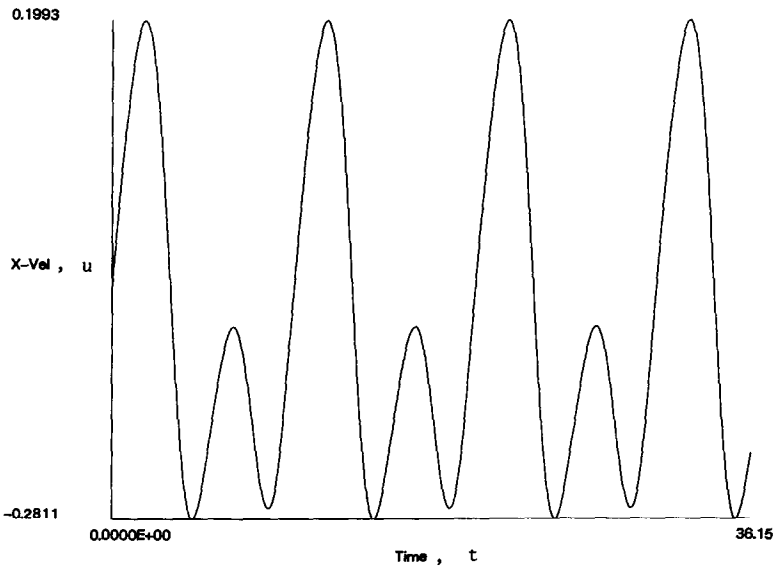

FIG. 10(a).

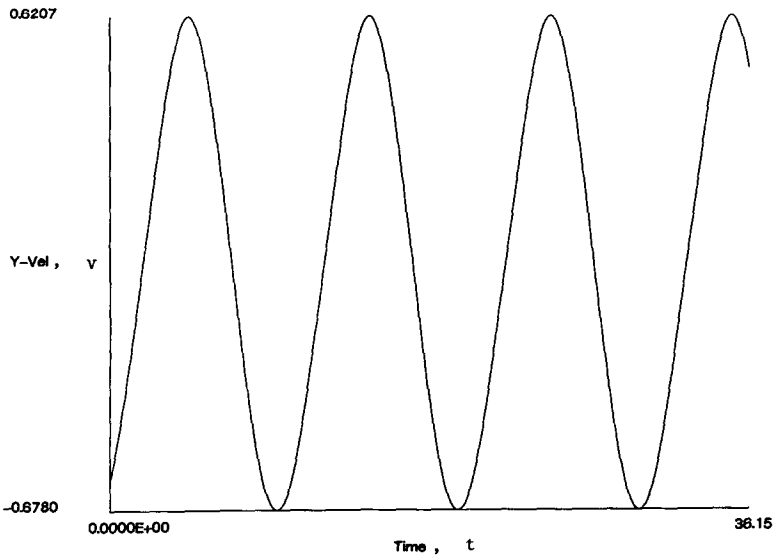

FIG. 10(b).

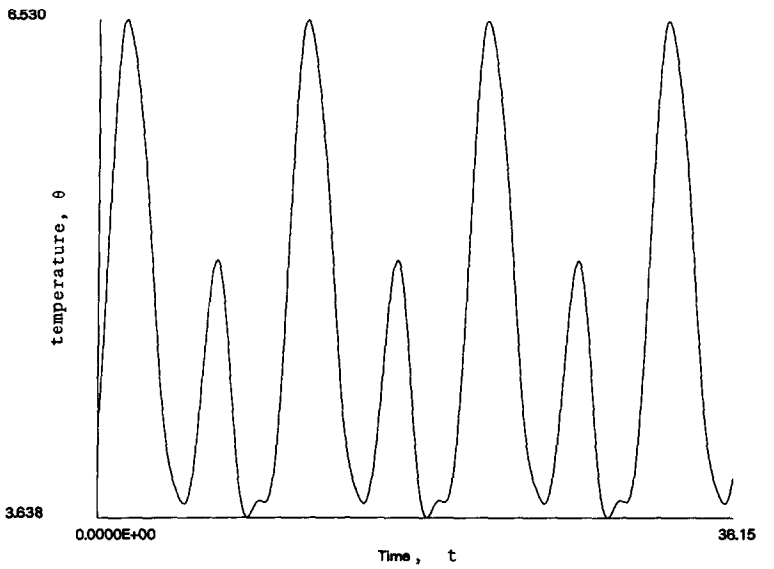

FIG. 10(c).

FIG. 10. Time history for $Re = 150$ and $Pr = 0.70$ of x-velocity (a) y-velocity (b) and temperature (c) at a point located $0.92D$ from the rear stagnation point and $0.068D$ above the centerline.

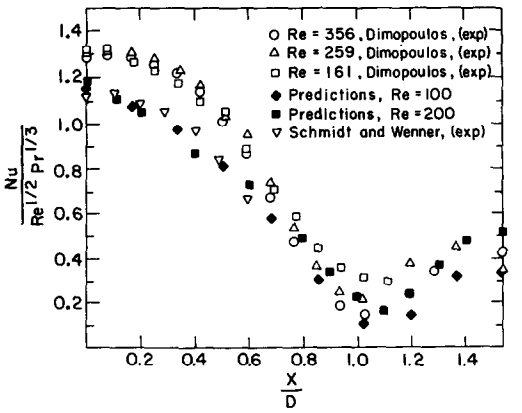

FIG. 11. Distribution of time-averaged heat transfer rate around the cylinder; comparison with experiment.

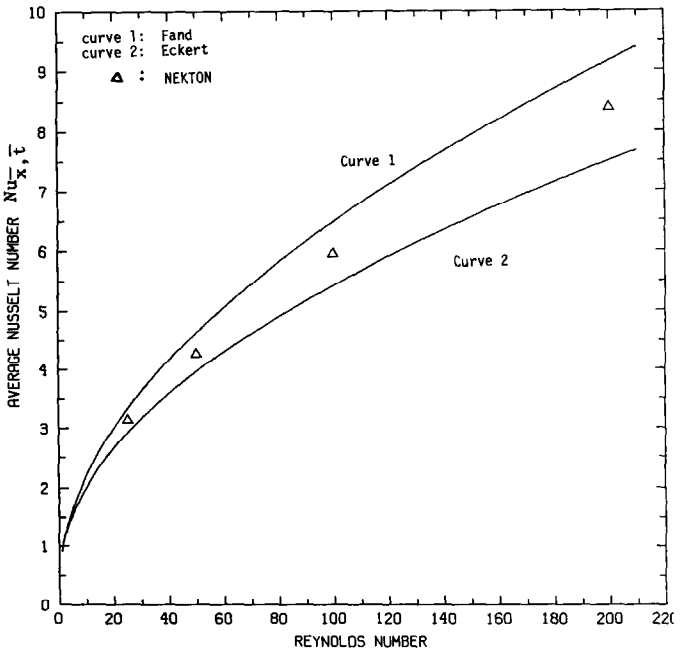

FIG. 12. Average Nusselt number vs Reynolds number; comparison with empirical formulas [6, 26].

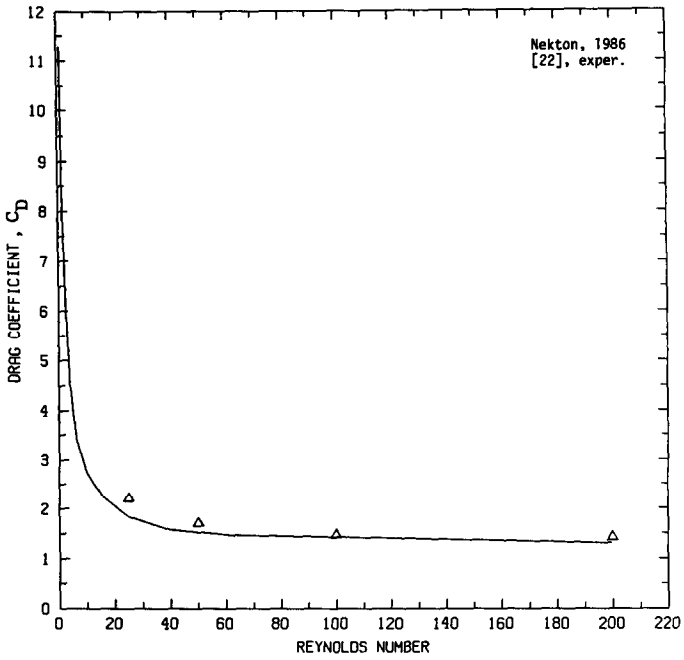

FIG. 13. Cylinder drag coefficient vs Reynolds number; comparison with experimental results [22].

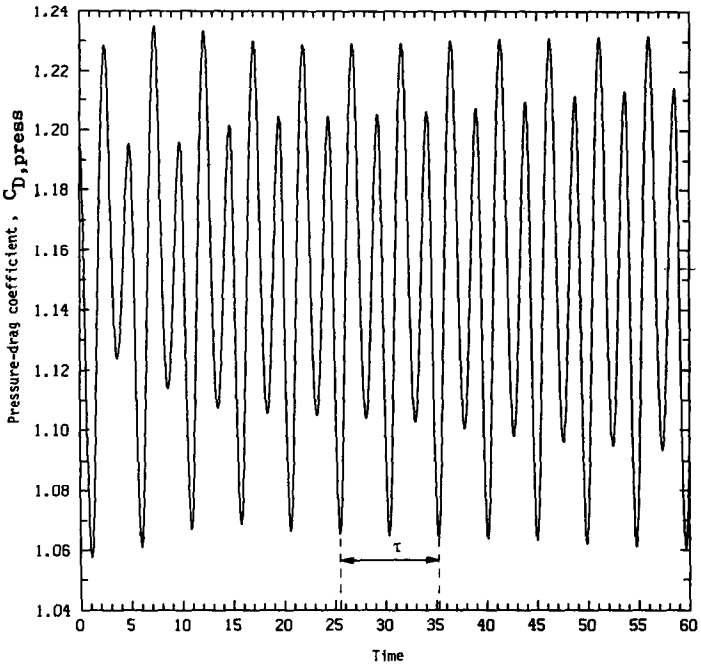

FIG. 14(a). The pressure component of cylinder drag as a function of time for $Re = 200$; note the presence of higher harmonics.

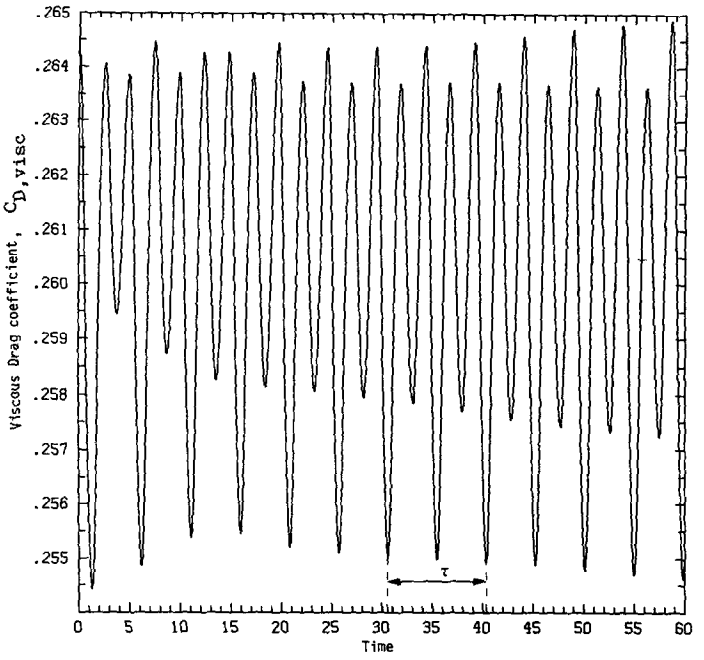

FIG. 14(b). The viscous component of cylinder drag as a function of time for $Re = 200$; higher harmonics are present here, too.

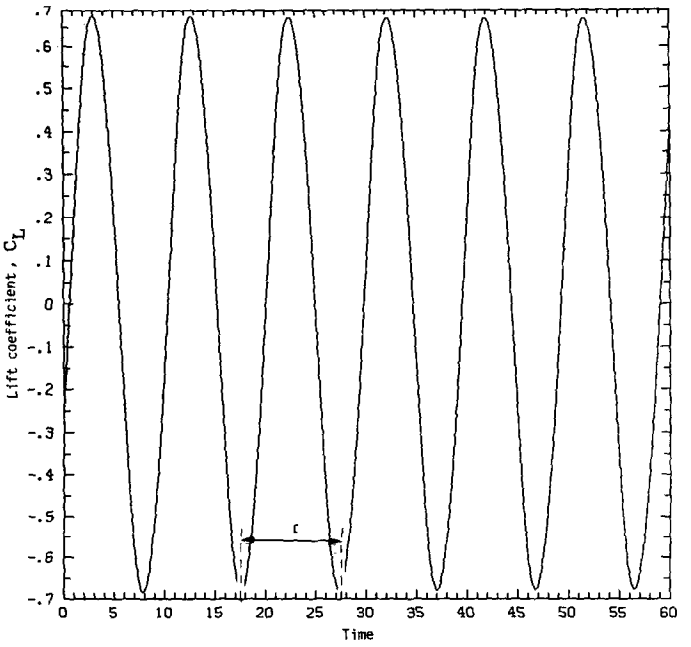

FIG. 15. Cylinder lift coefficient vs time for $Re = 200$.

Fig. 15, which oscillates with the fundamental frequency. More specifically, the drag coefficient oscillates with period $\tau/2$ and has a higher frequency component corresponding to $\tau/4$ in its signal. The space-averaged Nusselt number also exhibits similar behavior as the drag coefficient [25]. The explanation for this is that whereas the Nusselt number and the drag coefficient cannot distinguish between events that occur on the top and bottom of the cylinder, the lift coefficient (force in the y-direction) can.

Acknowledgements—I would like to acknowledge Professors A. T. Patera, B. B. Mikic and E. R. Eckert for their comments concerning this work. This work was supported by the National Science Foundation under Grant CBT 85-06146 and by the Office of Naval Research and DARPA under Contract N00014-85-K-0208.

REFERENCES

1. H. Bènard, Formation de centres de giration a l'arriere d'un obstacle en mouvement, *Compte Rendu* **147,** 839 (1908).
2. Th. von Karman, Ueber den Mechanisms des Widerstandes den ein bewgter Korper in einer Flussigkeit erfahrt, *Gott. Nachr.* 509 (1911).
3. J. L. Nayler and R. A. Frayzer, Vortex motion. Preliminary report upon an experimental method of investigating, by the aid of kinematograph photography, the history of eddying flow past a model immersed in water, Advisory Committee for Aeronautics, R & M (new series), No. 332 (1917).
4. E. Schmidt and K. Wenner, Heat transfer over the circumference of the heated cylinder in transverse flow, NACA-TM-1050 (1941).
5. A. Zukauskas and J. Ziugzda, *Heat Transfer of a Cylinder in Crossflow*. Hemisphere, Washington, D.C. (1986).
6. R. M. Fand, Heat transfer from a cylinder to water in crossflow, *Int. J. Heat Mass Transfer* **8,** 995 (1965).
7. U. C. Saxena and A. D. V. Laird, Heat transfer from a cylinder oscillating in a crossflow, *Trans. Am. Soc. Mech. Engrs*, Series C **100,** 684 (1978).
8. K. Sreenivasan and A. Ramachandran, Effect of vibration on heat transfer from a horizontal cylinder to a normal air stream, *Int. J. Heat Mass Transfer* **3,** 60 (1961).
9. D. B. Spalding and W. M. Pun, A review of methods for predicting heat transfer coefficients for laminar uniform property boundary layer flows, *Int. J. Heat Mass Transfer* **5,** 239 (1962).
10. C. E. Andraka and T. E. Diller, Heat transfer distribution around a cylinder in pulsating crossflow, *Trans. ASME* **107,** 976 (1985).
11. NEKTON User's Manual, Nektonics Inc., Bedford, Massachusetts (1986).
12. A. T. Patera, A spectral element method for fluid dynamics; laminar flow in a channel expansion, *J. Comp. Phys.* **54,** 468 (1984).
13. G. E. Karniadakis, E. T. Bullister and A. T. Patera, A spectral element method for solution of the two- and three-dimensional time-dependent incompressible Navier–Stokes equations, *Proc. Int. Symp. on Finite Element Methods for Nonlinear Problems*, Trondheim, Norway, p. 805. Springer, Berlin (1985).
14. N. K. Ghaddar, G. E. Karniadakis and A. T. Patera, A conservative isoparametric spectral element method for forced convection; application to fully developed flow in periodic geometries, *Numer. Heat Transfer* **9,** 277 (1986).
15. H. Honji and S. Taneda, Unsteady flow past a circular cylinder, *J. Phys. Soc. Japan* **27,** 1688 (1969).
16. W. M. Collins and S. C. R. Dennis, Flow past an impulsively started circular cylinder, *J. Fluid Mech.* **60,** 105 (1973).
17. J. H. Gerrard, The wakes of cylindrical bluff bodies at low Reynolds number, *Proc. R. Soc. Lond.* **A289,** 351 (1978).
18. P. M. Gresho, S. T. Chan, R. L. Lee and C. D. Upson, A modified Finite Element Method for solving the time-dependent incompressible Navier–Stokes equations. Part 2: applications, *Int. J. Numer. Meth. Fluids* **4,** 619 (1984).
19. E. R. G. Eckert and E. Soehngen, Distribution of heat transfer coefficients around circular cylinders in crossflow at Reynolds number from 20 to 500, *Trans. ASME* **75,** 343 (1953).
20. K. M. Krall and E. R. G. Eckert, Heat transfer to a transverse circular cylinder at low Reynolds number including rarefaction effects, *Proc. Int. Heat Transfer Conf.* **3,** FC6–FC9 (1970).
21. H. G. Dimopoulos and T. Hanratty, Velocity gradients at the wall for flow around a cylinder for Reynolds numbers between 60 and 360, *J. Fluid Mech.* **33,** 303 (1968).
22. D. J. Tritton, Experiments on the flow past a circular cylinder at low Reynolds numbers, *J. Fluid Mech.* **6,** 547 (1959).
23. M. Braza, P. Chassaing and H. H. Minh, Numerical study and physical analysis of the pressure and velocity fields in the near wake of a circular cylinder, *J. Fluid Mech.* **165,** 79 (1986).
24. M. M. Zdravkovich, Smoke observations of a Karman vortex street, *J. Fluid Mech.* **39,** 491 (1969).
25. G. E. Karniadakis, B. B. Mikic and A. T. Patera, Unsteady heat transfer from a cylinder in crossflow; a direct numerical simulation, Eighth International Heat Transfer Conference, Vol. 2, p. 429 (1986).
26. E. R. Eckert and R. M. Drake, *Analysis of Heat and Mass Transfer*. McGraw-Hill, New York (1972).

SIMULATION NUMERIQUE DE LA CONVECTION THERMIQUE FORCEE AUTOUR D'UN CYLINDRE EN ATTAQUE TRANSVERSALE

Résumé—La convection thermique forcée autour d'un cylindre en attaque transversale est étudiée, pour un nombre de Reynolds allant jusqu'à 200, par simulation numérique directe des équations de Navier–Stokes et d'énergie en utilisant la méthode spectrale. Les prédictions numériques de la dimension du sillage, de la structure temporelle et spatiale de l'allée de tourbillons de von Karman, des coefficients variables de portance, de trainée et de transfert thermique local; sont tous en excellent accord avec les données expérimentales disponibles. Différentes conditions limites pour le champ de vitesse externe sont utilisées pour tenir compte de l'étendue illimitée du domaine, tandis que sont simulées pour le champ de température, les conditions de flux de chaleur uniforme ou de température constante sur le cylindre.

NUMERISCHE SIMULATION DES WÄRMEÜBERGANGS BEI ERZWUNGENER QUERANSTRÖMUNG EINES ZYLINDERS

Zusammenfassung—Es wird der Wärmeübergang bei erzwungener Queranströmung eines einzelnen Zylinders für Reynolds-Zahlen oberhalb 200 durch numerische Simulation der Navier–Stokes'schen und der Energiegleichungen mit Hilfe der Spektral-Element-Methode untersucht. Die numerischen Vorhersagen für die Größe des Nachlaufbereichs, für die zeitliche und räumliche Struktur der von Karman'schen Wirbelstraße, für die instationären Auftriebs- und Widerstandskoeffizienten und für den lokalen instationären Wärmeübergangskoeffizienten stimmen sehr gut mit den verfügbaren experimentellen Daten überein. Zur Berücksichtigung des unendlich ausgedehnten Strömungsgebiets werden bei der Berechnung des Geschwindigkeitsfelds verschiedene Randbedingungen herangezogen, während für das Temperaturfeld die Randbedingungen 1. und 2. Art simuliert werden.

ЧИСЛЕННОЕ МОДЕЛИРОВАНИЕ ТЕПЛООТДАЧИ ПОПЕРЕЧНО ОБТЕКАЕМОГО ЦИЛИНДРА ПРИ ВЫНУЖДЕННОЙ КОНВЕКЦИИ

Аннотация—Методом прямого численного моделирования уравнений Навье–Стокса и уравнений энергии с использованием спектрального метода элементов исследована теплоотдача поперечно обтекаемого одиночного цилиндра при вынужденной конвекции для значений числа Рейнольдса до 200. Результаты численных расчетов размера следа, временной и пространственной структуры вихревой дорожки Кармана, нестационарного коэффициента подъемной силы, лобового сопротивления и локального коэффициента нестационарного теплообмена хорошо согласуются с имеющимися экспериментальными данными. Для учета неограниченного характера расчетной области используются различные граничные условия для поля скорости, в то время как для температурного поля моделируются условия равномерного теплового потока и постоянной температуры цилиндра.